Quantum Scattering Calculations of the $O(^1D) + N_2(X^1\Sigma_g^+) \rightarrow O(^3P) + N_2(X^1\Sigma_g^+)$ Spin-Forbidden Electronic Quenching Collision

Toshiyuki Takayanagi

Advanced Science Research Center, Japan Atomic Energy Research Institute, Tokai, Ibaraki 319-1195, Japan

Received: January 9, 2002; In Final Form: March 1, 2002

Three-dimensional quantum scattering calculations have been carried out for the $O(^1D) + N_2 \rightarrow O(^3P) + N_2$ spin-forbidden electronic quenching process using a simplified collision model, in which only the lowest singlet surface and one triplet surface are taken into account. The standard close-coupling technique has been used to obtain nonadiabatic transition probabilities, and the coupled-state approximation was applied to calculate the total quenching cross section. Previously developed analytical potential energy surfaces and the spin−orbit coupling element have been employed. The results of the close-coupling calculations have been compared to the results of the quasiclassical trajectory surface hopping method. Two versions of the method have been used; one uses Tully's fewest switches algorithm, and the other is the hopping method of Preston and Tully. It has been found that both of the trajectory surface hopping methods give too large quenching probabilities compared to those of the quantum results, in which the quenching dynamics is exclusively resonance-dominated. Detailed analyses of the quantum results show that a curve crossing picture cannot be employed to describe the present nonadiabatic collision. The calculated quenching cross sections have been also compared to those of experimental data as well as previous theoretical results.

1. Introduction

The spin-forbidden electronic quenching collision, $O(^1D) + N_2(X^1\Sigma_g^+) \rightarrow O(^3P) + N_2(X^1\Sigma_g^+)$, is a very important process in the upper atmosphere and has consequently been the subject of both experimental and theoretical studies. The $O(^1D)$ atoms are produced in the photodissociation processes of O_2 and O_3 molecules by the sunlight in the ultraviolet and vacuum-ultraviolet regions.[1] Since the $O(^1D)$ atoms produced by the above photodissociation processes are highly translationally excited, the translational relaxation process, fast-$O(^1D) + N_2 \rightarrow$ slow-$O(^1D) + N_2$, also plays an important role in the upper atmosphere.[1] It should be emphasized that both the spin-forbidden electronic quenching collision and the translational relaxation process compete and occur under the superthermal condition.

Matsumi et al.[2−4] have recently reported various aspects of the $O(^1D) + N_2 \rightarrow O(^3P) + N_2$ collision using a laser technique. They have measured the nascent fine structure distribution of $O(^3P_{J=2,1,0})$ by vacuum-ultraviolet laser-induced fluorescence.[2] They have also found that the electronic energy transfer efficiency to the internal (vibrational + rotational) energy of N_2 is about 30 ± 7% by measuring the Doppler profile of the product $O(^3P_J)$ atom.[2] This value agrees with the previous experimental value[5] 33 ± 10% which was obtained from indirect measurements, although collision energies were somewhat different between both experiments. Speed and angular relaxation processes induced by collisions with N_2 for the velocity of superthermal $O(^1D)$ photofragments have been studied using the same experimental technique.[3] Moreover, Matsumi and Chowdhury[4] have recently measured the collision energy dependence of the cross section of the $O(^1D) + N_2 \rightarrow O(^3P) + N_2$ process and showed that the cross section at the high collision energy 8 ± 6 kcal/mol is about 5 times smaller than that at thermal condition at room temperature.

Since the $O(^1D) + N_2 \rightarrow O(^3P) + N_2$ collision is one of the simplest examples of the electronically nonadiabatic processes including potential surfaces with different spin multiplicities, extensive theoretical studies have previously been carried out.[6−19] It is clear that the relevant interaction causing the spin-forbidden transition is spin−orbit coupling between the singlet and triplet states. The first attempt to find singlet−triplet crossing surfaces and to obtain the spin−orbit coupling elements from accurate ab initio electronic structure calculations has been performed by Chang and Yarkony.[12] They have characterized the potential energy surfaces in the vicinity of the singlet−triplet crossing using a large-scale multireference configuration interaction (MRCI) method and then calculated the spin−orbit couplings using the full Breit−Pauli operator. They have found that the maximum value of the spin−orbit coupling is about 90 cm^{-1}. Tachikawa et al.[13] have carried out ab initio calculations by the Møller−Plesset second-order perturbation method (MP2) for both the lowest singlet and triplet states. Nakamura and Kato[15,16] have recently carried out extensive ab initio electronic structure calculations at the multiconfigurational quasidegenerate perturbation (MCQDPT) level of theory and then constructed global potential energy functions for the lowest singlet states and the lowest two triplet states. They have also calculated many points of the spin−orbit coupling matrix elements and fitted the calculated points to analytical functions. They have carried out quantum dynamics calculations for the $N_2O(^1\Sigma^+) \rightarrow N_2(^1\Sigma_g^+) + O(^3P)$ spin-forbidden predissociation reaction using the developed analytical surfaces. More recently, Hwang and Mebel[18] have carried out ab initio calculations for the N_2O-$(^1\Sigma^+) \rightarrow N_2(^1\Sigma_g^+) + O(^3P)$ process at various levels of theory and characterized local minima and transition states on the lowest singlet and triplet potential energy surfaces.

In addition to the ab initio electronic structure studies, as mentioned above, several dynamics studies have also been reported for the $O(^1D) + N_2 \rightarrow O(^3P) + N_2$ process; however,

10.1021/jp0200425 CCC: $22.00
Published on Web 04/17/2002

most of these previous studies employed theoretical methods based on classical dynamics. Theoretical treatments performed by Tully[8] and Zahr et al.[9] assume that a collision complex is formed on the lowest singlet N_2O potential surface and that the weak spin−orbit interaction can induce electronic quenching to the triplet states with an essentially unit probability, since the intersection of the singlet and triplet surfaces is crossed many times during the life of the collision complex. The classical trajectory method as well as the statistical approximation was employed in their studies. They have found that the electronic quenching probability decreases with increasing collision energy. The above-mentioned electronic quenching mechanism has recently been confirmed in trajectory surface hopping calculations by Tachikawa et al.[13,14] They have also calculated the vibrational and rotational distributions of N_2 produced from the $O(^1D) + N_2 \rightarrow O(^3P) + N_2$ process. Nakamura and Kato[16] have recently performed the first quantum dynamics calculations for the $N_2O \rightarrow N_2 + O(^3P)$ spin-forbidden predissociation process on the ab initio potential energy surfaces. They have obtained a total of 1692 vibrational states on the lowest $1^1A'$ surface for zero total angular momentum by diagonalizing the singlet Hamiltonian matrix and then calculated the decay rate of an individual singlet vibrational resonance state to the $^3A'$ state using the Fermi golden rule combined with the time-dependent wave packet method. Although they gave a clear quantum mechanical picture for the $N_2O \rightarrow N_2 + O(^3P)$ unimolecular process, they did not provide any information for the $O(^1D) + N_2 \rightarrow O(^3P) + N_2$ quenching process, since their calculations have been carried out below the $N_2 + O(^1D)$ threshold.

Motivated by the current status, as mentioned above, in this paper we present three-dimensional quantum mechanical scattering calculations for the spin-forbidden electronic quenching collision, $O(^1D) + N_2 \rightarrow O(^3P) + N_2$. As mentioned previously, the collision complex and the subsequent nonadiabatic transition model have been widely accepted for this process. However, we should notice that the metastable collision complex corresponds to the resonant quasibound state trapped in the deep potential well of the $1^1A'$ N_2O surface. In addition, electronically nonadiabatic transitions are well-known quantum mechanical phenomena. Both facts suggest that we must employ quantum scattering methods in order to fully understand the quenching mechanism of the $O(^1D) + N_2 \rightarrow O(^3P) + N_2$ collision. We also compare quantum scattering results to trajectory surface hopping results and discuss the validity of this semiclassical method.

2. Computational Methods

A. Collision Model and Potential Energy Surfaces for $O(^1D) + N_2 \rightarrow O(^3P) + N_2$. To accurately describe the $O(^1D) + N_2 \rightarrow O(^3P) + N_2$ spin-forbidden collision system, one has to consider 14 potential energy surfaces, since the $O(^1D)$ state is 5-fold degenerate and the $O(^3P)$ state is 9-fold degenerate including spin multiplicity. Also, all singlet−triplet and triplet−triplet spin−orbit coupling elements should be taken into account. Using modern ab initio electronic structure codes, one can calculate all potential energy surfaces as well as spin−orbit matrix elements at a fairly accurate level in principle. In fact, Hoffmann and Schatz[20] have recently carried out ab initio calculations of the spin−orbit matrix elements for the $O(^1D) + H_2 \rightarrow O(^3P) + H_2$ system. However, we here considered a simplified model consisting of only the lowest singlet surface ($1^1A'$) and one triplet surface ($1^3A'$) similar to all of the previous theoretical studies.[8,13−16] This is also because the main purpose of the present work is to obtain a qualitative quantum mechanical picture of electronically nonadiabatic spin-forbidden collisions as well as to compare quantum scattering results with trajectory surface hopping results. It should, however, be emphasized that all triplet surfaces that asymptotically correlate to $O(^3P_J) + N_2$ must be included in the dynamics calculation in order to calculate spin−orbit fine structure distributions for $O(^3P_{J=2,1,0})$. In fact, Matsumi et al.[2] have experimentally measured the fine structure distributions for the $O(^1D) + N_2 \rightarrow O(^3P_J) + N_2$ collision using a vacuum-ultraviolet laser-induced fluorescence technique. We cannot obtain such fine structure distributions from the present simplified collision model. Soon, however, we will present all spin−orbit matrix elements using the ab initio electronic structure method, and we are in the midst of such calculations.

To perform scattering calculations based on the simplified collision model, as mentioned above, we need two potential energy surfaces. Recently, several analytical potential energy surfaces[13,16,17] for the lowest singlet state have been developed on the basis of accurate ab initio calculations. In the present calculations, we employ the potential surface of Nakamura and Kato.[16] Their surface has been constructed on the basis of extensive ab initio calculations at the level of the multiconfigurational quasidegenerate perturbation (MCQDPT) theory with a triple-ζ plus double polarization basis set. A total of 1160 ab initio points were then used for constructing the analytical surface, where the double-many-body-expansion (DMBE)[21] type function was employed. They have developed two versions of the singlet surface, and we here employ their DMBE2 surface for dynamics calculations. We also employ the semiempirical model potential energy surface of Zahr et al.[9] for comparison. Zahr et al.[9] have developed two versions of model potential surfaces; one is the surface which includes translational−rotational coupling but not translational−vibrational coupling, and the other includes both couplings. We here employ the latter surface, since it is more realistic and this surface has been employed in previous studies.[9,10] This surface is denoted as ZPM2 hereafter in this paper. For the triplet state, we employed an analytical function of Nakamura and Kato,[16] which is a fit to the ab initio points for the $^3A'$ state calculated at the MCQDPT level of theory. Nakamura and Kato[16] have also given an analytical function for the spin−orbit coupling element, which has been calculated at the state-averaged complete active space self-consistent field level of theory. After averaging the calculated spin−orbit elements over $M_s = -1, 0, 1$, where M_s is the spin projection quantum number, they have constructed an analytical function by fitting the ab initio calculated values to a Gaussian type function. We also performed dynamics calculations using the constant spin−orbit coupling (80 cm^{-1}), since most of the previous dynamics studies[9,13−15] assumed the spin−orbit coupling to be independent of coordinates. Here, we will examine this effect on electronically nonadiabatic dynamics.

Contour plots of the singlet surfaces, triplet surface, and spin−orbit coupling element employed in the present study are given in Figure 1 as a function of Jacobi coordinates, R, r, and γ (see below for definition). The zero energy is set to the potential bottom of the asymptotic $O(^3P) + N_2$ channel. The experimental energy difference (45.4 kcal/mol) between the $O(^1D)$ and $O(^3P)$ states is used to set the difference between the asymptotes of the surfaces. For collinear configurations ($\gamma = 0°$) it is seen that a general feature of both the DMBE2 and ZPM2 surfaces is quite similar, but it should be noted that the DMBE2 surface has a small bottleneck at $R \sim 5a_0$; that is, a saddle point occurs with a barrier height of about 0.7 kcal/mol. On the other hand, the ZPM2 surface has no saddle point. For T-shaped configura-

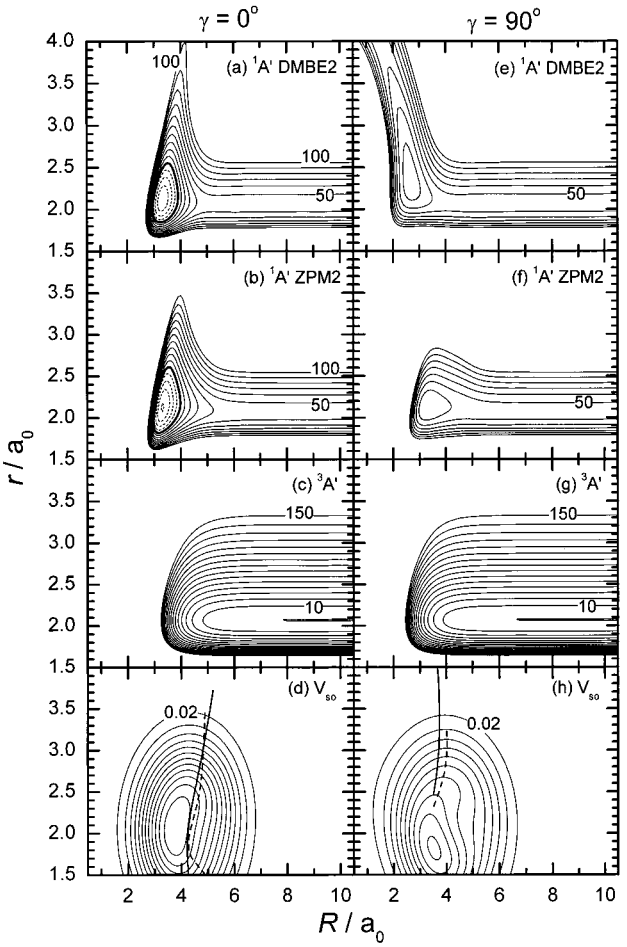

Figure 1. Contour plots of the singlet and triplet potential energy surfaces (a−c and e−g) and the spin−orbit coupling element (d and h) employed in scattering calculations as a function of Jacobi coordinates (R, r, γ). Contours are spaced by 10 kcal/mol for potential surfaces while being spaced 0.02 kcal/mol for spin−orbit coupling. Solid curves are used for energies that are positive relative to the $O(^3P) + N_2$ potential bottom, dashed curves are used for negative energies, and bold lines denote zero-energy contours. Bold solid lines in d and h are the crossing seams between the $^1A'$-DMBE2 and $^3A'$ surfaces, while bold dashed lines are those between the $^1A'$-ZPM2 and $^3A'$ surfaces.

tions ($\gamma = 90°$), a somewhat different behavior is seen between the DMBE2 and ZMP2 surfaces. Also plotted in Figure 1d,h are the crossing seams between the singlet and triplet surfaces. It is seen that the location of the crossing seam is quite similar for both the DMBE2 and ZPM2 surfaces. It can also be seen that the spin−orbit interaction for collinear configurations is somewhat larger than that for T-shaped configurations.

B. Close-Coupling Calculations. The time-independent Schrödinger equations for two-surface atom−diatom collision systems in a diabatic representation can generally be written as

$$T\begin{pmatrix}\varphi_1\\ \varphi_2\end{pmatrix}+\begin{pmatrix}V_{11} & V_{12}\\ V_{12} & V_{22}\end{pmatrix}\begin{pmatrix}\varphi_1\\ \varphi_2\end{pmatrix}=E\begin{pmatrix}\varphi_1\\ \varphi_2\end{pmatrix} \qquad (1)$$

where T and E are the kinetic energy operator and the total energy, respectively. V_{ij} is the diabatic potential energy matrix element. In the present case, V_{11} corresponds to the singlet potential energy surface while V_{22} corresponds to the triplet surface. V_{12} is the spin−orbit coupling matrix element. φ_i is the wave function, and the index i refers to the manifold of diabatic states. We employ the standard Jacobi coordinate system (R, r, γ) to describe the collision of an atom A and a diatomic molecule BC, where R, r, and γ are the distance between A and the center of mass of BC, the internuclear distance of BC, and the angle between R and r, respectively. Using the Jacobi coordinates, the kinetic energy T can be explicitly given by (in atomic unit)

$$T = -\frac{1}{2\mu}\frac{\partial^2}{\partial R^2} - \frac{1}{2m}\frac{\partial^2}{\partial r^2} + \frac{(J-j)^2}{2\mu R^2} + \frac{j^2}{2mr^2} \qquad (2)$$

where μ and m are the reduced mass between A and BC and the reduced mass of BC, respectively. J and j are the total angular momentum and the rotational angular momentum associated with the rotation of BC, respectively. In the present study, we introduced the coupled-state (centrifugal sudden) approximation[22,23] for computational simplicity by ignoring the Colioris coupling term; that is, the $(J - j)^2$ term was simply replaced by $[J(J + 1) - 2K^2 + j^2]$, where K is the projection of J on the body-fixed axis R. Also, we completely neglected the effect of electronic Colioris coupling.[24]

To solve numerically the scattering Schrödinger equations, we employed a close-coupling technique by expanding the wave function in terms of the diatomic eigenfunctions of N_2, as (dropping the electronic manifold index)

$$\varphi(R, r, \gamma) = \sum_{v,j} \chi_{vj}(R)\, \phi_{vj}(r)\, f_{jK}(\gamma) \qquad (3)$$

where $\phi_{vj}(r)$ and $f_{jK}(\gamma)$ are the vibrational and rotational eigenfunctions, respectively, and $\chi_{vj}(R)$ is the expansion coefficient. $\phi_{vj}(r)$ can be obtained from the solution of the following one-dimensional eigenvalue problem:

$$\left(-\frac{1}{2m}\frac{\mathrm{d}^2}{\mathrm{d}r^2} + \frac{j(j+1)}{2mr^2} + V_{\mathrm{ref}}(r)\right)\phi_{vj}(r) = \epsilon_{vj}\phi_{vj}(r) \qquad (4)$$

Here $V_{\mathrm{ref}}(r)$ is the N_2 diatomic potential energy. We have solved the eigenvalue problem using the discrete-variable-representation (DVR) method[25] with a particle-in-box basis set. Using this expansion, we can finally obtain the usual close-coupling equations. The resulting close-coupling equations were numerically solved using the standard renormalized Numerov method[26,27] with a usual boundary condition. The final scattering matrix elements can be obtained by applying boundary conditions in the asymptotic region.[27]

Numerical parameters were carefully chosen such that calculated results were converged within a few percent. Extensive convergence tests were carried out by changing the number of sectors in R, the number of channels, and the DVR basis set parameters. Finally, a total of 1000 sectors in the range $R = 2.5-17.5a_0$ with a fixed step size and 300 channels (200 for the singlet state and 100 for the triplet state) were found to be necessary to obtain numerically converged scattering matrix elements in the total energy range ($E_{\mathrm{tot}} < 3$ eV) considered in this work. For the DVR calculations, we employed 200 DVR points in the range $1.5a_0 < r < 4.0a_0$. All of the close-coupling calculations were carried out using a Fujitsu VPP5000 supercomputer. In the normalized Numerov method, a matrix inversion (order of 300) should be done at each sector (1000 sectors). It took less than 10 min/energy using a fully vectorized computer code. Since a dense grid of the energy (∼20 000 points) was necessary to obtain detailed resonance structures, actual calculations were carried out using a parallel technique (32 processors).

C. Trajectory Surface Hopping Calculations. Classical dynamics calculations employing the trajectory surface hopping

(TSH) method[28] were carried out for comparison. Two types of TSH methods which are based on different hopping schemes were used in this work. One is Tully's fewest switches (TFS) method,[29] and the other is the TSH method of Preston and Tully.[30]

In the TFS method,[29] similar to the standard quasiclassical trajectory method on a single potential energy surface, nuclear motions are calculated by solving the classical Hamilton equations of motion. Trajectories were started with quantized vibrational and rotational energies and propagated on electronically adiabatic surfaces. In addition, complex electronic state coefficients were simultaneously integrated. An electronically nonadiabatic transition is possible at every time step. The momenta were adjusted in the direction of the nonadiabatic coupling vector. Although the method to remove classically forbidden transitions has recently been proposed,[31] we here employed Tully's original algorithm for computational simplicity. Numerical integration was carried out using the standard fourth-order Runge−Kutta method with a fixed time increment (1−2 atomic time unit, 1 au = 2.419×10^{-17} s).

In the TSH method, due to Preston and Tully,[30] the surface hopping is allowed only on the crossing seam. During each trajectory, the energy difference between the singlet and triplet states was monitored. If the sign of the energy difference is changed, we go back to the previous point, reduce the time increment by a factor of 10, and more precisely find the crossing point. At the crossing point found, the nonadiabatic hopping probability was calculated by the standard Landau−Zener formula. Integration of the classical equations of motion was carried out with the Runge−Kutta method similar to the TFS calculations.

For each of the two TSH methods, we calculated 2000−4000 trajectories for each value of the total energy, the initial vibrational and rotational quantum numbers, and the initial impact parameter.

3. Results and Discussion

Figure 2 presents the $J = 0$ total quenching probabilities for the $O(^1D) + N_2(v = j = 0) \rightarrow O(^3P) + N_2$ collision as a function of the translational energy. The probabilities are summed over all of the final vibrational and rotational states of N_2. Since the initial rotational state of N_2 is zero, the impact parameters are also zero in the trajectory calculations. We have performed three sets of calculations. Figure 2a shows the results in which the DMBE2 surface was used for the singlet state, while Figure 2b shows the ZPM2 surface result. In Figure 2c, the ZPM2 surface was used, but the spin−orbit interaction was set to the constant value of 80 cm^{-1}. At first, we compare the quantum close-coupling results to the TSH results. We can see that the quenching probabilities calculated from the close-coupling method are completely dominated by resonances in this collision energy range. At low collision energies, the quenching probability suddenly rises to large values, where the energy hits one of the resonance energies. At off-resonance energies, the quenching probability is small at low collision energies, but the contribution of resonances becomes small with the energy increases. This means that there is an essentially minor contribution of direct processes in the low energy range and the collision dynamics is completely controlled by resonances which play the role of a gatekeeper for the quenching process. On the other hand, at high collision energies (>15 kcal/mol) the fluctuation due to resonances is somewhat small; however, we can still see a rich structure of resonance.

It can be seen that both the TFS and TSH results are much larger than the quantum results for all three types of calculations,

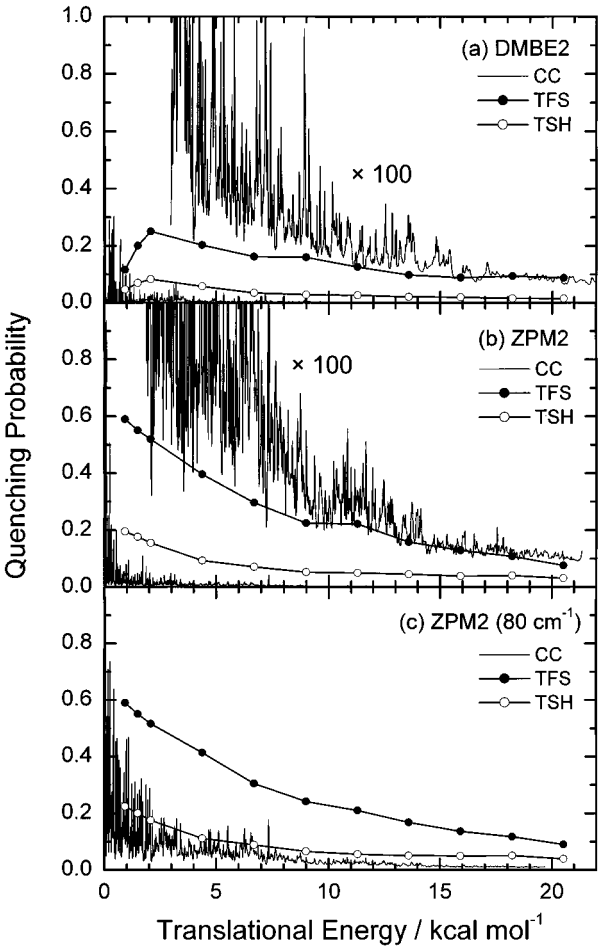

Figure 2. Total electronic quenching probability of the $O(^1D) + N_2(v = j = 0) \rightarrow O(^3P) + N_2$ process for $J = 0$ as a function of the translational energy: (a) the results calculated using the DMBE2 surface for the singlet state, (b) the ZPM2 surface results, and (c) the ZPM2 surface results but with the constant spin−orbit coupling (80 cm^{-1}). Solid lines correspond to the quantum close-coupling results, solid lines with solid circles correspond to the TFS results, and solid lines with open circles correspond to the TSH results. For the quantum calculations, magnified results are also plotted.

where the latter TSH term denotes the TSH method of Preston and Tully. No resonance structure can be seen in either of the TFS and TSH results, as expected, simply because the classical dynamics cannot describe quantum mechanical effects such as resonance. However, it is interesting to note that the DMBE2 results give broad peaks around the collision energy 2 kcal/mol, while for the results using the ZPM2 surface the calculated probability monotonically decreases with the increase of the collision energy. Therefore, we can conclude that the broad peaks are due to the fact that the DMBE2 surface has a very small barrier, as mentioned in the previous section (see Figure 1). It should also be emphasized that the TFS method gives larger quenching probabilities than the TSH method by a factor of about 3 in this collision energy range. Such a large difference between the TFS and TSH results was seen in our previous study[32] on the electronically nonadiabatic reaction of $D + H_2^+ \rightarrow DH + H^+$, $D^+ + H_2$, and $DH^+ + H$, where the results of the accurate quantum reactive scattering calculations have been compared to both the TFS and TSH results. In that study, we found that the TSH method gives very small nonadiabatic transition probabilities similar to the present case. This significant difference is due to the difference in the hopping mechanism between the TFS and TSH methods. In the TSH method

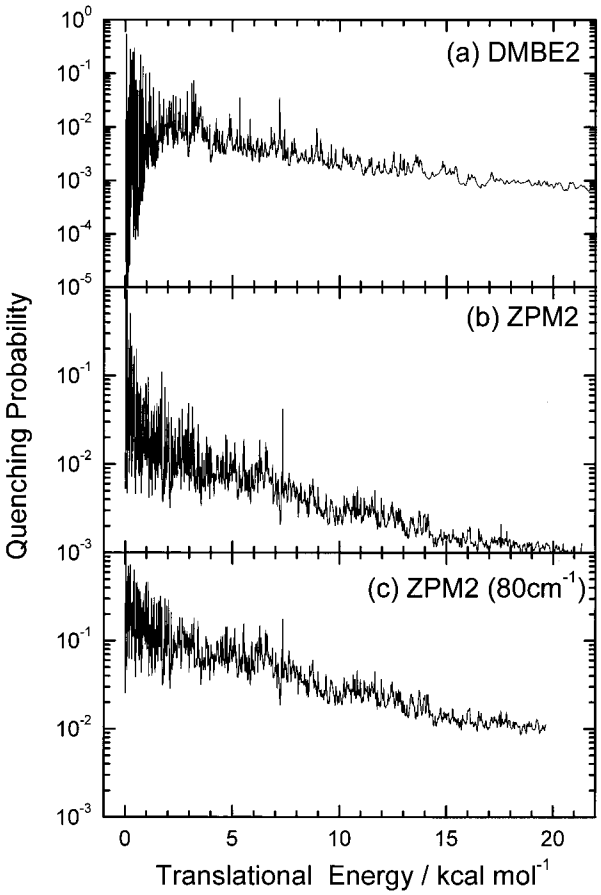

Figure 3. Same as Figure 2, but with probabilities plotted in a logarithmic scale showing only the quantum close-coupling results.

of Preston and Tully, nonadiabatic hopping is allowed only at the crossing seams, while nonadiabatic hopping can take place slightly away from the avoided crossing in the TFS method. Nevertheless, it should be emphasized again that neither the TFS nor TSH method gives reliable quenching probabilities.

Next, we compare the quantum results of three types of calculations. Figure 3 shows the same quenching probabilities as those in Figure 2, but plotted in a logarithmic scale for clarity. It is seen that the translational energy dependence of the probability for the DMBE2 results is different from that of the ZPM2 results at low energies. Similar to the TSH and TFS results plotted in Figure 2a, a broad maximum is seen at an energy of 2−3 kcal/mol for the DMBE2 result, while no energy threshold behavior is seen for the ZPM2 results. Above this energy, if we ignored the resonance fine structures, the calculated quenching probabilities monotonically decrease with the increase of the translational energy for all three results. However, we should notice that a significant difference is seen for the absolute value of probability. It is interesting to note that the quenching probability calculated with the ZPM2 surface and the constant spin−orbit coupling is much larger than those of the other two results. For example, both DMBE2 and ZPM2 results using the spin−orbit function of Nakamura and Kato give a probability of about 10^{-3} at the translational energy 20 kcal/mol. On the other hand, the corresponding value is 10^{-2} for the constant spin−orbit result and is larger by a factor of 10. This result indicates that the functional form of the spin−orbit coupling plays a very important role for the present nonadiabatic process.

To qualitatively understand the sensitivity of the spin−orbit interaction to the quenching probabilities, we plot adiabatic

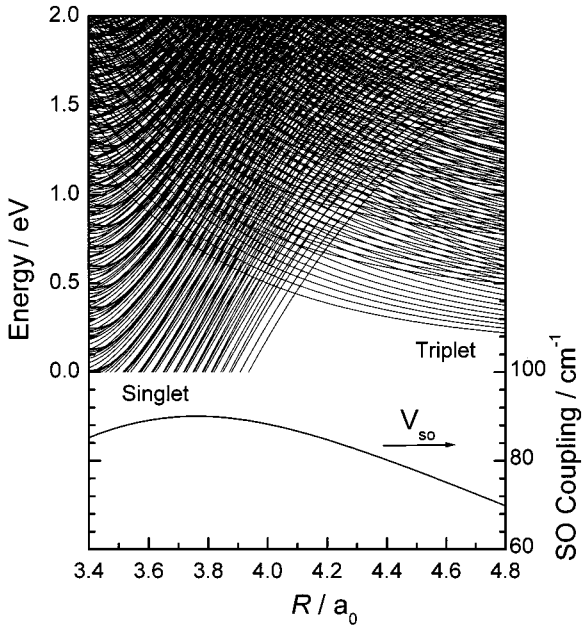

Figure 4. Adiabatic eigenvalues plotted as a function of the Jacobi scattering coordinate *R*. Also plotted is the spin−orbit coupling along *R*.

eigenvalues as a function of the Jacobi scattering coordinate *R* in Figure 4. These eigenvalues were obtained by diagonalizing the $J = 0$ Hamiltonian with a basis set of asymptotic rovibrational wave functions. The crossing between the singlet and triplet potential surfaces occurs at $R \sim 4a_0$ (see Figure 1); however, we can see a large number of avoided crossings in the adiabatic curves in the range $3.4a_0 < R < 4.6a_0$. This is simply because the $O-N_2$ system has many vibrational and rotational states due to its large masses. For a multidimensional case such as the present collision system, we have to take all important crossing points into account for describing electronically nonadiabatic transitions. The importance of the crossing points, of course, depends on the spin−orbit coupling; that is, the crossing points where the spin−orbit interaction is large should be more important than those where the interaction is small. Thus, it may be probable that the overall quenching probability depends on the functional form of the spin−orbit interaction. However, since the spin−orbit interaction is very weakly dependent on the coordinates as shown in Figure 4, it is unlikely that the constant spin−orbit interaction drastically enhances the quenching process by a factor of 10. Thus, we have to look for another reason.

To do so, we look for differences in the resonance structures in detail, comparing the ZPM2 results with the spin−orbit interaction of Nakamura and Kato and the ZPM2 results with the 80 cm^{-1} constant spin−orbit coupling. Figure 5 shows the $J = 0$ quenching probabilities for the $O(^1D) + N_2(v = j = 0) \rightarrow O(^3P) + N_2$ process as a function of the translational energy just above the $O(^1D) + N_2(v = j = 0)$ threshold. Note that only a narrow energy range (0−0.2 kcal/mol) is plotted so that we can identify an individual resonance. First, we can see that the positions of resonance remain almost unchanged for both sets of calculations. This result simply indicates that the resonance position is determined only by the singlet potential energy surface. On the other hand, the resonance widths are significantly different between the two sets of calculations; the results with the constant spin−orbit coupling have much broader resonance structures. This observation implies that the spin−orbit coupling drastically affects the lifetime of the resonances at least for this

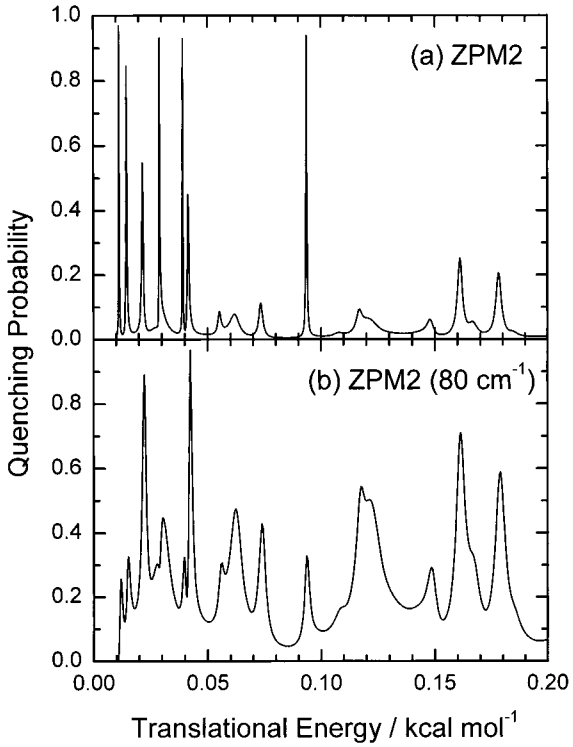

Figure 5. Total electronic quenching probability of the $O(^1D) + N_2(v = j = 0) \rightarrow O(^3P) + N_2$ process for $J = 0$ as a function of the translational energy in a very narrow energy region: (a) the results with the ZPM2 surface and the spin−orbit coupling of Nakamura and Kato and (b) the results with the ZPM2 surface and the 80 cm^{-1} constant spin−orbit coupling.

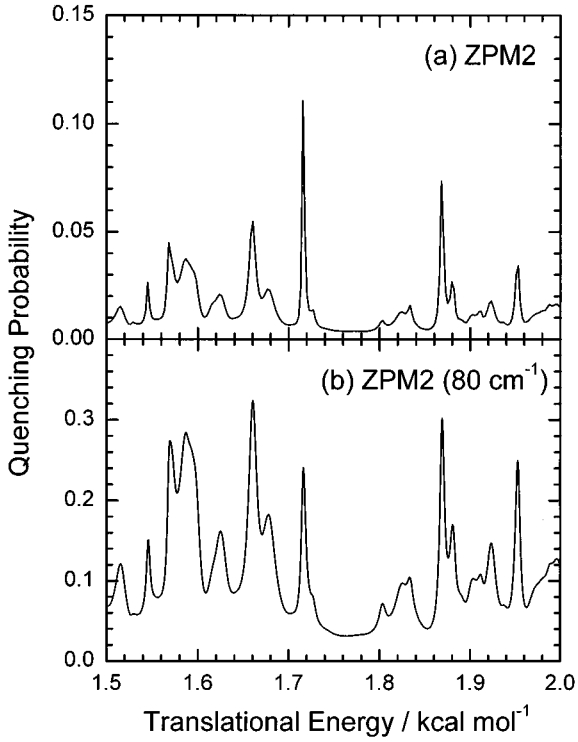

Figure 6. Same as Figure 5, but within the energy region 1.5−2.0 kcal mol^{-1}.

small energy region. This is because the resonances are essentially isolated and sharp in this region. As the energy increases, a somewhat different behavior was seen. Figures 6 and 7 show the quenching probability in the energy ranges 1.5−2.0 and 14−17 kcal/mol, respectively. In these energy ranges,

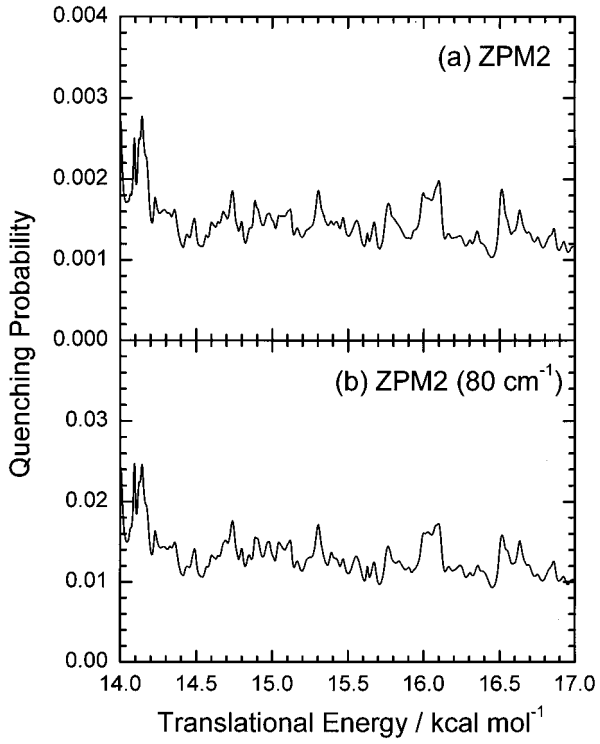

Figure 7. Same as Figure 5, but within the energy region 14.0−17.0 kcal mol^{-1}.

the resonance line widths for the two sets of calculations are seen to give similar probability curves, although the absolute values of the quenching probabilities are very different. This suggests that, in the higher energy region, the resonances are overlapping each other and the lifetimes are not sensitive to the functional form of the spin−orbit interaction but are determined mainly by the singlet surface. However, it should be noted that the overall quenching probability calculated with the 80 cm^{-1} constant spin−orbit interaction is much larger than that calculated with the spin−orbit coupling of Nakamura and Kato, since the baseline in Figure 6b or 7b is much larger than that in Figure 6a or 7a. All of these findings naturally lead to the conclusion that the curve crossing picture, presented in Figure 4, cannot be employed to understand the $O(^1D) + N_2 \rightarrow O(^3P) + N_2$ spin-forbidden electronic quenching process. It can be concluded that electronically nonadiabatic transition probabilities are very sensitive to both the resonance wave function on the singlet surface and the functional form of the spin−orbit coupling. The present computational results also suggest that the coupled-channel distorted-wave approximation[27,33,34] can be applied to the present system for relatively high energies, where the nonadiabatic transition probability is small. Such a calculation was previously carried out for the $Ar^+ + N_2 \rightarrow Ar + N_2^+$ nonadiabatic charge-transfer collision.[34] Consequently, we can conclude that the overall quenching probability strongly depends on both the shape of the singlet potential energy surface and the shape of the singlet−triplet spin−orbit interaction. Since this kind of sensitivity has not been found in the TSH calculations at all, such sensitivity should be due to the quantum mechanical nature of the $O(^1D) + N_2 \rightarrow O(^3P) + N_2$ spin-forbidden electronic quenching process.

Although the collision model in this work has been quite simplified, as mentioned previously, it should be informative to calculate the total quenching cross sections and compare them to available experimental results. We have calculated the quenching cross sections for $O(^1D) + N_2(v = j = 0) \rightarrow O(^3P) + N_2$ by changing the value of the total angular momentum J.

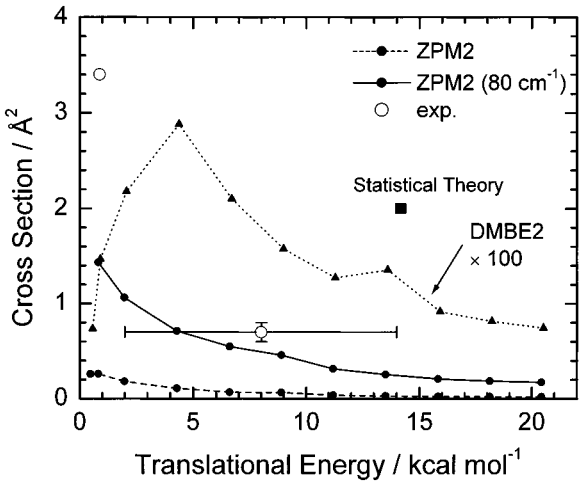

Figure 8. Total electronic quenching cross section for the $O(^1D) + N_2 \rightarrow O(^3P) + N_2$ process as a function of the translational energy. Open circles with and without the error bar are experimental data taken from ref 4 (see text for detail). The dotted line with solid triangles and the dashed line with solid circles correspond to the close-coupling results calculated using the DMBE2 and ZPM2 surfaces, respectively, with the Nakamura−Kato spin−orbit coupling. The solid line with solid circles is the close-coupling result with the ZPM2 surface and the constant spin−orbit coupling. The solid square is taken from ref 9.

To obtain the converged cross sections, we have carried out the scattering calculations up to $J = 250$ but only at selected values of the translational energy due to computational costs. Although it would be very interesting to see if the resonance structure seen in the $J = 0$ probabilities persists for the quenching cross section, this issue is beyond the present purpose. In Figure 8, we compare the calculated cross sections to the experimental results as well as a previous value reported by Zahr et al.[9] Only two experimental points are available. The quenching cross section has been reported to be 0.7 ± 0.1 Å^2 at an energy of 8 ± 6 kcal/mol by Matsumi and Chowdhury.[4] The large error bar in the translational energy is due to the fact that their experiment was carried out in a gas cell and not in a molecular beam. A cross section of 3.4 Å^2 at an energy of ~1 kcal/mol was estimated from the thermal rate constant[35] ($k = 2.6 \times 10^{-11}$ cm^3 molecule^{-1} s^{-1}) at room temperature using the relation $k = \langle v \rangle \sigma$, where $\langle v \rangle$ is the average velocity and σ is the cross section. Also plotted (2 Å at 14 kcal/mol) in Figure 8 is the result calculated with the statistical theory by Zhar et el.[9] Note that all theoretical results are including a factor of $^1/_5$, which accounts for the electronic degeneracy of the $O(^1D)$ state. It can be seen that both the DMBE2 and ZPM2 results calculated with the spin−orbit coupling of Nakamura and Kato give much smaller cross sections. As seen in the calculated quenching probability for $J = 0$, the DMBE2 result has a broad maximum at an energy of about 5 kcal/mol and this is typical for the case that the potential surface has a barrier. It is interesting to note that the ZPM2 result using the constant spin−orbit coupling gives reasonable agreement with the experimental data, although the calculated result seems to be somewhat small. The statistical result of Zahr et al. is too large, and this suggests that the cross sections calculated with the TSH (TFS) method would be too large, although we did not calculate the cross sections using the TSH method. To carry out a more quantitative comparison, further experimental studies will be necessary. In addition, such experiments would definitely stimulate further theoretical studies including accurate determination of the potential energy surfaces as well as the spin−orbit coupling matrix elements.

4. Summary and Conclusions

We have carried out three-dimensional quantum scattering calculations for the $O(^1D) + N_2 \rightarrow O(^3P) + N_2$ spin-forbidden electronic quenching process, using a simplified collision model including the lowest singlet surface and one triplet surface. The standard close-coupling technique and the coupled-state approximation[22,23] have been employed to obtain electronic quenching probabilities and cross sections. Two analytical potential energy surface functions have been used for the singlet state; one is the potential surface of Nakamura and Kato[15,16] which was developed on the basis of accurate ab initio electronic structure calculations, and the other is the semiempirical one of Zahr et al.[9] For the triplet state, the analytical surface of Nakamura and Kato[16] based on the ab initio calculations has been employed. We have also used both the analytical function of Nakamura and Kato[16] and the constant value for the singlet−triplet spin−orbit coupling element. The TSH calculations including two different hopping schemes have been carried out for comparison; one is the TSH method of Preston and Tully,[30] where nonadiabatic surface hopping is allowed only at the surface crossing seams, and the other is the TFS method.

The electronic quenching probabilities calculated with the quantum close-coupling method show that the dynamics is exclusively resonance-dominated. We have found that the TSH methods give larger quenching probabilities compared to those in the quantum close-coupling results. The TSH results do not strongly depend on the choice of the singlet potential energy surface nor spin−orbit interaction. In the case of the quantum results, however, we found that the electronic quenching probability is very sensitive to the shape of the potential energy surfaces as well as the shape of the singlet−triplet spin−orbit interaction. This result implies that a simple curve crossing picture cannot be employed for describing the nonadiabatic quenching dynamics. The total quenching cross sections have been calculated and compared to experimental results. Although the general quantum picture for the $O(^1D) + N_2 \rightarrow O(^3P) + N_2$ spin-forbidden electronic quenching process can be understood in terms of quantum mechanical resonance, as mentioned above, further quantitative studies including accurate determinations of both the singlet and triplet potential energy surfaces and spin−orbit coupling matrix elements would be needed in order to obtain more accurate cross sections. In particular, all spin−orbit matrix elements depending on the value of spin-projection quantum number (M_s) should be calculated to obtain the fine structure distribution of $O(^3P_J)$ as well as vibrational and rotational state distributions of N_2. Such a theoretical study is currently underway in our research group.

Acknowledgment. The author would like to thank Dr. H. Tachikawa, Dr. A. Wada, Dr. H. Akagi, and Dr. M. Shiga for useful discussions. The author also thanks Dr. T. Suzuki, Dr. T. Kohguchi, Dr. S. Nanbu, and Dr. M. Aoyagi for valuable comments.

References and Notes

(1) Manabe, S.; Strickler, R. J. *J. Atmos. Sci.* **1964**, *21*, 361.
(2) Matsumi, Y.; Inagaki, Y.; Morley, G. P.; Kawasaki, M. *J. Chem. Phys.* **1994**, *100*, 315.
(3) Matsumi, Y.; Shamsuddin, S. M.; Sato, Y.; Kawasaki, M. *J. Chem. Phys.* **1994**, *101*, 9610.
(4) Matsumi, Y.; Chowdhury, A. M. S. *J. Chem. Phys.* **1996**, *104*, 7036.
(5) Schofield, K. *J. Photochem.* **1978**, *9*, 55.
(6) Fisher, E. R.; Bauer, E. *J. Chem. Phys.* **1972**, *57*, 1966.
(7) Delos, J. B. *J. Chem. Phys.* **1973**, *59*, 2365.
(8) Tully, J. C. *J. Chem. Phys.* **1974**, *61*, 61.

(9) Zahr, G. E.; Preston, R. K.; Miller, W. H. *J. Chem. Phys*. **1975**, *62*, 1127.
(10) Marks, A. J.; Thompson, D. L. *J. Chem. Phys.* **1980**, *95*, 8056.
(11) Hopper, D. G. *J. Chem. Phys.* **1984**, *80*, 4290.
(12) Chang, A. H. H.; Yarkony, D. R. *J. Chem. Phys*. **1993**, *99*, 6824.
(13) Tachikawa, H.; Hamabayashi, T.; Yoshida, H. *J. Phys. Chem*. **1995**, *99*, 16630.
(14) Tachikawa, H.; Ohnishi, K.; Hamabayashi, T.; Yoshida, H. *J. Phys. Chem*. **1997**, *101*, 2229.
(15) Nakamura, H.; Kato, S. *Chem. Phys. Lett.* **1998**, *297*, 187.
(16) Nakamura, H.; Kato, S. *J. Chem. Phys*. **1999**, *110*, 9937.
(17) González, M.; Valero, R.; Sayós, R. *J. Chem. Phys.* **2000**, *113*, 10983.
(18) Hwang, D.-Y.; Mebel, A. M. *Chem. Phys*. **2000**, *89*, 259.
(19) Teule, J. M.; Groenenboom, G. C.; Neyer, D. W.; Chandler, D. W.; Janssen, M. H. M. *Chem. Phys. Lett*. **2000**, *320*, 177.
(20) Hoffmann, M. R.; Schatz, G. C. *J. Chem. Phys*. **2000**, *113*, 9456.
(21) Pastrana, M. R.; Quantales, L. A. M.; Brandão, J.; Varandas, A. J. C. *J. Phys. Chem*. **1990**, *94*, 8073.
(22) Pack, R. T. *J. Chem. Phys.* **1974**, *60*, 633.
(23) McGuire, P.; Kouri, D. J. *J. Chem. Phys*. **1974**, *60*, 2488.
(24) Drukker, K.; Schatz, G. C. *J. Chem. Phys*. **1999**, *111*, 2451.
(25) Light, J. C.; Hamilton, I. P.; Lill, J. V. *J. Chem. Phys*. **1985**, *82*, 1400.
(26) Johnson, B. R. *J. Chem. Phys.* **1977**, *67*, 4086.
(27) Hubbard, L. M.; Shi, S.; Miller, W. H. *J. Chem. Phys*. **1983**, *78*, 2381.
(28) Chapman, S. *Adv. Chem. Phys*. **1992**, *82*, 187.
(29) Tully, J. C. *J. Chem. Phys*. **1990**, *93*, 1061.
(30) Preston, R. K.; Tully, J. C. *J. Chem. Phys*. **1971**, *54*, 4297.
(31) Fang, J.-Y.; Hammes-Schiffer, S. *J. Chem. Phys*. **1999**, *110*, 11166.
(32) Takayanagi, T.; Kurosaki, Y.; Ichihara, A. *J. Chem. Phys*. **2000**, *112*, 2615.
(33) Schatz, G. C.; Hubbard, L. M.; Dardi, P. S.; Miller, W. H. *J. Chem. Phys*. **1984**, *81*, 231.
(34) Clary, D. C.; Sonnenfroh, D. M. *J. Chem. Phys*. **1989**, *90*, 1686.
(35) DeMore, W. B.; Sander, S. P.; Golden, D. M.; Hampson, R. F.; Kurylo, M. J.; Howard, C. J.; Ravishankara, A. R.; Kolb, C. E.; Molina, M. *Chemical Kinetics and Photochemical Data for Use in Stratosphere Modeling*; JPL Publication No. 94-26; Jet Propulsion Laboratory: Pasadena, CA, 1994.